JPE 17-3-25

https://doi.org/10.6113/JPE.2017.17.3.835
ISSN(Print): 1598-2092 / ISSN(Online): 2093-4718

Standardized Design of the Transmitting Coils in Inductive Coupled Endoscope Robot Driving Systems

Quan Ke†, Pingping Jiang*, and Guozheng Yan*

†,*Department of Instrument Science and Engineering, Shanghai Jiaotong University, Shanghai, China

Abstract

A transmitting coil with an optimal topology and number of turns can effectively improve the performance of the wireless power transfer (WPT) systems for endoscope robots. This study proposes the evaluation parameters of the transmitting coils related to the performance of the WPT system to standardize the design of the transmitting coils. It considers both the quality factor of transmitting coils and the coupling factor between the two sides. Furthermore, an analytical model of transmitting coils with different topologies is built to exactly estimate the evaluation parameters. Several coils with the specified topologies are wound to verify the analytical model and the feasibility of evaluation parameters. In the case of a constant power received, the related evaluation parameters are proportional to the transfer efficiency of the WPT system. Therefore, the applicable frequency ranges of transmitting coils with different topologies are determined theoretically. Then a transmitting coil with a diameter of 69 cm is re-optimized both theoretically and experimentally. The transfer efficiency of the WPT system is increased from 3.58% to 7.37% with the maximum magnetic field intensity permitted by human tissue. Finally, the standardized design of the transmitting coil is achieved by summing-up and facilitating the optimization of the coils in various situations.

Key words: Endoscope robot, Litz-wire transmitting coil, Standardized design, Wireless power transfer

I. INTRODUCTION

Capsule endoscopic has drawn a lot of attention within the scope of biomedical engineering since Given Imaging Ltd launched the PillCam in 2001 [1]-[4]. The capsule locomotes along with the intestinal peristalsis, which increases the failure rate of disease detection. Therefore, Endoscopic Micro-Robots (EMR) have gradually become the development trend of endoscopes [5], [6]. Because of the active motion of EMRs, more energy is consumed and an adequate power supply has become an urgent issue to be settled.

Nowadays, mid-range inductive coupled wireless power transfer systems have been adopted in EMR systems [7]-[10]. Generally, the transmitter generates a one-dimensional uniform magnetic field, and the receiver inside the EMR uses a three-dimensional receiving coil to mitigate the impact of variations in the position and orientation of robot. Instead of Helmholtz coils, this study uses a solenoid pair as a transmitting coil to increase the intensity of the magnetic field while keeping its homogeneity [11]-[14]. The diameter of the solenoid pair has been increased to 69 cm to suit the complete inspection of the gastrointestinal tract [14]. Then the important parameters to quantitatively evaluate an inductive link are negatively affected, such as the power delivered to the load P_L and especially the transfer efficiency η.

In weakly coupled WPT systems, the high quality factor of the coil pairs allows for efficient telemetric energy transfer [14]-[16]. Optimization of the transmitter can be realized by using several topologies of winding transmitting coils, including spaced windings, and a multi-wire coil with an arbitrary number of parallel wires and layers [17]. Although typical values are relatively small, the coupling factor between two coils k_{12} changes significantly and has to be considered. First, suitable evaluation parameters related to η and P_L should be achieved to standardize the design of the transmitting coils.

Manuscript received Aug. 25, 2016; accepted Jan. 21, 2017
Recommended for publication by Associate Editor Hao Ma.
†Corresponding Author: kequanhubei@163.com
Tel: +86-18221015751, Shanghai Jiaotong University
*Dept. of Instruments Science and Eng., Shanghai Jiaotong Univ., China

Depending on specific implements, η is quantified by many formulas correlated with the mutual inductance. By definition, the influence of the transmitting coils on the mutual inductance of the inductive links is reflected in the intensity of the magnetic field generated at the receiving coil with a driving current of 1A [18]. Like Helmholtz coils, the magnetic field intensity at the center of the solenoid pairs is proportional to the ampere turns of the coils [24]. Within the workspace of an EMR, the quantitative expressions of η and P_L are simplified, and the evaluation parameters of the transmitter are obtained, while taking k_{12} into account.

In addition, an analytical model of the transmitting coils with different topologies should be built to facilitate the design process. It should include three lumped parameters: the inductance L, the stray capacitance C_s, and the ac resistance R_{ac}. Based on [15] and [19]-[21], the analytical expressions of L and C_s can be derived. As for R_{ac}, the exact two dimension solution is available [14].

Utilizing the evaluation parameters and the analytical model, the applicable frequency range of the different topologies for transmitting coils can be achieved. Under the preconditions of satisfying the energy demand of EMR systems, the optimal topology and number of turns are determined theoretically and experimentally for a solenoid pair in [14]. The re-optimized transmitting coil effectively improves the performance of WPT systems for EMRs. Accordingly, this optimization process can serve as a standard.

This paper is organized as follows. Section II introduces the basis of WPT systems for EMRs, and deduces the evaluation parameters of the transmitting coils. The available topologies for the transmitting coils are proposed in Section III, and the magnetic field intensity at the centre of coils with different topologies is given. In section IV, an analytic model of the transmitting coils is built for different topologies. Section V verifies the analytic model and evaluation parameters derived by experiments. Through theoretical analysis and experiments in section VI, the optimization of the transmitting coil with a diameter of 69 cm is achieved. In addition, the standard design of the transmitting coils is formed. Results and conclusion are provided in section VII.

II. The Basis of WPT Systems for EMR

The weakly coupled WPT systems for EMRs are realized by the magnetic coupling technique. Both sides of the WPT system need to be compensated by capacitors to improve η, and a series resonance circuit is preferred on account of its better load performance [22]. First, this section quantitatively gives the value of η for WPT systems. Then by analysing the mutual inductance of two coils, the effects of parameters of the transmitting coils on the performance of WPT systems are theoretically derived.

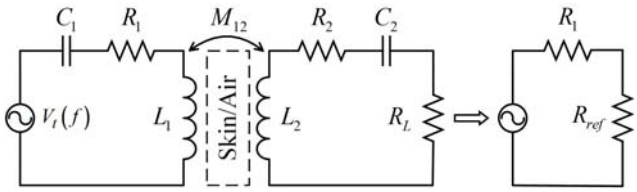

Fig. 1. (a) Equivalent circuit of a WPT system for an EMR; (b) equivalent circuit of a load reflected onto the transmitting side.

A. Transfer Efficiency of WPT Systems

Fig. 1(a) shows a simplified schematic diagram of a 2-coil inductive link for an EMR. The highest η can be achieved when the coils are tuned at the operating frequency of the WPT system, f_o. The value of f_o, which is mainly determined by the receiving side, is set to 220 KHz based on experiments in [14]. The effect of the receiving sides on the transmitting sides at resonance can be modelled with the reflecting impedance, which is calculated by:

$$R_{ref} = \frac{\omega^2 M_{12}^2}{R_2 + R_L} = k_{12}^2 Q_1 R_1 Q_{2L} \tag{1}$$

where $k_{12} = M_{12}/\sqrt{L_1 L_2}$ is the coupling factor, $Q_1 = \omega L_1 / R_1$, and $Q_{2L} = \omega L_2/(R_2 + R_L)$. In addition, R_1 includes the equivalent resistance of the transmitting circuit. Later, the transmitting side at resonance can be simplified as shown in Fig. 1(b). Since it is in series with R_1, R_{ref} determines P_L. Due to the large transfer distance, $K_{12}^2 Q_1 Q_2 \ll 1$, the value of η for this inductive coupled system can be given as follows:

$$\eta \approx k_{12}^2 Q_1 Q_{2L} \cdot \frac{R_L}{R_2 + R_L} = \frac{\omega^2 M_{12}^2}{R_1 (R_2 + R_L)} \cdot \frac{R_L}{R_2 + R_L} \tag{2}$$

which concurs with the results in [14], [22]. The quantitative expression of M_{12} should be proposed to illustrate the effect of the transmitting coils on the value of η in Equ. (2).

B. Mutual Inductance

The mutual inductance between two coils is defined as the total flux linking one coil per unit of change in current in the other coil. The solenoid pair generated a uniform magnetic field in the axial direction within the workspace of the EMR. Therefore, for the sake of simplicity, the receiving coil is placed in the centre of the solenoid pair and the axes of both coils are perfectly aligned. In this way, the mutual inductance, when the solenoid acts as a receiving coil and a cylindrical rod with relative permeability μ_r, is inserted [18]:

$$M_{12} = H_c \cdot n_r \pi r_r^2 \cdot \frac{\mu_0 \mu_r}{1 + D_{fc}(\mu_r - 1)} = H_c \cdot F_r \tag{3}$$

where r_r and n_r are the radius in meters and the number of turns of the receiving coils, D_{fc} is the demagnetizing factor, and H_c is the intensity of the magnetic field at the center of a transmitting coil with a driving current of 1A.

Despite the different types of ferrite cores utilized in receiving coils, the derived analytical expression of mutual inductance remains appropriate with the equivalent μ_r and D_{fc} [8]-[14]. μ_r is an intrinsic property of magnetic materials, and closely related to the magnetic field around the receiving coil at the frequency of f_o. Thus, the impact of the solenoid pairs on M_{12} is solely determined by H_c.

C. Evaluation Parameters

The evaluation parameters of transmitting coils related to the values of η and P_L for WPT systems provide support for the optimal design of transmitting coils. Substituting Equ. (3) into Equ. (2), the contribution of the transmitting coils on η can be obtained by:

$$\eta \approx \frac{H_c^2}{R_1} \cdot \frac{\omega^2 R_L}{\left(R_2 + R_L\right)^2} \cdot F_r^2 \tag{4}$$

Evidently, instead of Q_1, the ratio H_c^2/R_1 can serve as an evaluation parameter on η, and takes k_{12} into account. P_L is defined as the input power $I_d^2 R_1$ multiplied by η, and it can be expressed as:

$$P_L \approx I_d^2 H_c^2 \cdot \frac{\omega^2 R_L}{\left(R_2 + R_L\right)^2} \cdot F_r^2 = H_{cd}^2 \cdot \frac{\omega^2 R_L F_r^2}{\left(R_2 + R_L\right)^2} \tag{5}$$

where H_{cd} is the intensity of a magnetic field generated at the centre of the coil axis with a driving current of I_d. To meet the energy required by EMR systems, the maximum H_{cd} should be considered, and that could be suitably regarded as another evaluation parameter.

Therefore, the optimal design of the transmitting coil can be achieved by enlarging H_c^2/R_1 on the premise of a high enough H_{cd} for the receiving side. To facilitate the design process, the analysis of H_c and the building of an analytical model of transmitting coils are both essential.

III. Transmitting Coils with Different Topologies

The solenoid pair in Fig. 2 has been determined by increasing Q_1 with an optimal number of turns [14]. However, the topologies of multi-wire coils, with parallel wires connected at both ends, will effectively enlarge Q_1 within a range of frequencies [17]. In addition, the topology of spaced winding increases the self-resonant frequency of the transmitting coil. Then it improves the performance of the WPT system at higher frequencies. The topologies to optimize the transmitting coils detailed in Fig. 3 have a significant impact on the coil dimensions. Therefore, the proposed evaluation parameters are suitable and persuasive, considering k_{12}. The main purpose of this section is to obtain

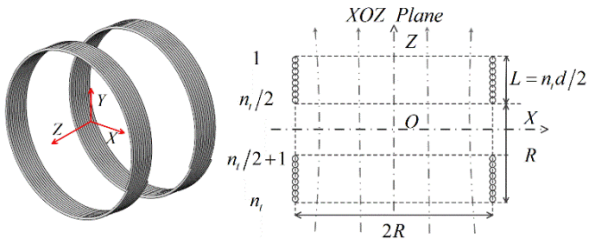

Fig. 2. Single-layer tightly wound transmitting coil structure.

an accurate expression of H_c for the solenoid pairs with different topologies.

Fig. 2 depicts the constructional features of the solenoid pairs. Assuming the center of coil is set to a point where $Z = 0$ and the symmetry axis of coil corresponds to Z, the H_c of the solenoid pairs can be given as:

$$H_c\left(z = 0, I = 1\right) = H\left(R/2 + z\right) + H\left(R/2 - z\right) \tag{6}$$

where $H(z)$ is the magnetic field intensity at a point on the symmetry axis of the solenoid tightly wound with a finite length L_t, and is expressed as [23]:

$$H(z) = \frac{nI}{2}\left(\frac{z + L_t/2}{\sqrt{R^2 + \left(z + L_t/2\right)^2}} - \frac{z - L_t/2}{\sqrt{R^2 + \left(z - L_t/2\right)^2}} \right) \tag{7}$$

where n represents the number of coil turns per unit length, and the diameter of the used wire is set to d.

Due to the large dimensions of the transmitting coils, the ratio $L_t/R \ll 1$. The value of H_c of the solenoid pair can be expanded in a Maclaurin's series of L_t/R, ignoring the high order terms:

$$H_c(z) \approx 0.71554 \frac{nL_t}{R} = 0.35777 \frac{n_t}{R} \tag{8}$$

The approximation of H_c in Equ. (8) is linearly related to the number of turns n_t, and consistent with that of the Helmholtz coil derived in [24].

However, the large pitch of the solenoid pairs with the topologies in Fig. 3 leads to a significant radial component of H_c and H_{cr}. According to the numerical calculation of the magnetic field on the axis of a helical current, H_{cr} increases with the pitch, but reduces with an increasing L_t [25]. To eliminate H_{cr} as much as possible, the pitch should be less than a critical value determined in the case of the solenoid pair with the shortest L_t. This study focuses on the re-optimization of the solenoid pair in [14]. Therefore, the minimum n_t is set to 16 and the diameter of the utilized Litz-wire is $d = 2$ mm [14]. Then the pitch of the solenoid pair with $L_t = 8d$ can be determined by a numerical analysis of H_c to ensure the ratio $H_{cr}/H_c \le 0.04$ [25]:

$$P_{tc} \le 0.0019 \cdot 2\pi R = 4.1186 \ (mm) \tag{9}$$

When the pitch varies within the range derived in Equ. (9),

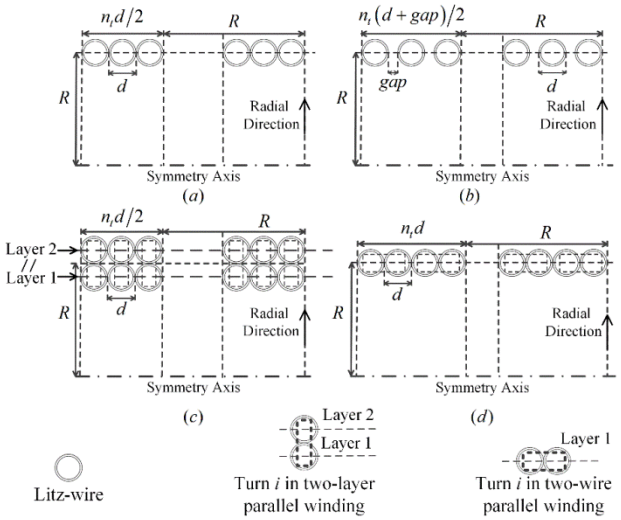

Fig. 3. Topologies of transmitting coils. (a) Single-layer tightly wound coil. (b) Coil with spaced winding. (c) Coil with parallel layer winding. (d) Coil with parallel wire winding.

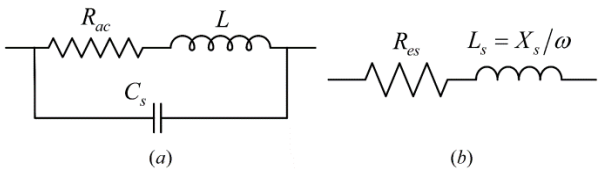

Fig. 4. (a) Lumped parameter equivalent circuit. (b) Equivalent circuit assumed by LCR meters.

each turn of the transmitting coils with different topologies can be regarded as a circular current, and the Equ. (8) is still available. The topology of multi-layer parallel winding leads to an increase of R. The transmitting coil with this topology can be considered as a single-layer coil with an equivalent radius R_z. To maintain an equal magnetic field intensity at the center of transmitting coils per unit length, R_z can be set as [26]:

$$R_z = \frac{R_{oc} - R_{ic}}{Ln(R_{oc}/R_{ic})} \tag{10}$$

where R_{ic} and R_{oc} are the inner and outer radius of transmitting coils with multi-layer parallel winding.

Within the constraint of the pitch, the topologies in Fig. 3 have little influence on H_c. The optimal topology of the transmitting coils has to reduce the equivalent series resistance (ESR) of the coils and simultaneously enlarge the driving current I_d at the frequency of f_o.

IV. Analytical Model of Transmitting Coils

The lumped parameter equivalent circuit of transmitting coils shown in Fig. 4(a) allows for an accurate representation of coil behavior over a wide frequency range. It consists of an inductance L, a stray capacitance C_s, and an ac resistance R_{ac}. To build the analytical model of transmitting coils with different topologies, the quantitative expressions of the lumped parameters are derived separately in this section. The lumped parameters model in Fig. 4(a) can usually be simplified as the series circuit of R_{es} and L_s in Fig. 4(b) assumed by LCR meters. R_{es} and L_s are obtained from Fig. 4(a) as follows:

$$Z_s = \frac{R_{ac} + j\omega L\left(1 - \omega^2 LC_s - R_{ac}^2 C_s/L\right)}{\left(1 - \omega^2 LC_s\right)^2 + \omega^2 C_s^2 R_{ac}^2} = R_{es} + j\omega L_s \tag{11}$$

where R_{es} is the ESR of the transmitting coil.

A. Inductance

The overall inductance of the transmitting coil includes all of the single-turn coils' self-inductances and the mutual inductances between different turns. In [19], the self-inductance of a single-loop with a radius of R_i and a wire radius of r_0 is given as:

$$L_s = \mu_0 R_i \left[\ln\left(\frac{8R_i}{r_0}\right) - 2 \right] \tag{12}$$

While for coils with multi-layer parallel winding, the thickness of the coils should be considered, and each turn can be treated as a thin disk coil. The self-inductance of single-turn coils with multi-layer parallel winding is given as [20]:

$$L_{sd} = \frac{\mu_0}{2\left(R_{oc} - R_{ic}\right)^2} \int_0^{\pi} \int_{R_{ic}}^{R_{oc}} \int_{R_{ic}}^{R_{oc}} \frac{r_1 r_2 \cdot \cos\theta \, d\theta \, dr_1 dr_2}{\sqrt{r_1^2 + r_2^2 - 2r_1 r_2 \cos\theta}} \tag{13}$$

where μ_0 is the permeability of vacuum. L_{sd} can be obtained as an analytical and in numerical form expressed over the complete elliptic integrals of the first and second kind and terms, which will be solved numerically [20].

Under the condition, $r_0/R \ll 1$, the mutual inductance of two turns with the radius R_i and R_j, and separated by d_r can be approximated as:

$$M(R_i, R_j, d_r) = \mu_0 \sqrt{R_i R_j} \left[\left(\frac{2}{k} - k\right) \mathrm{K}(k) - \frac{2}{k} \mathrm{E}(k) \right] \tag{14}$$

where:

$$k^2 = \frac{4R_i R_j}{(R_i + R_j)^2 + d_r^2}$$

and $\mathrm{K}(k)$ and $\mathrm{E}(k)$ are the complete elliptic integrals of the first and second kind, respectively [19]. On the basis of the filament method, the mutual inductance of two turns in coils with multi-layer parallel winding can be precisely obtained. To apply the filament method, as shown in Fig. 5, the single-loops with multi-layer parallel winding are subdivided into $(2N_c+1)\times(2N_c+1)$ cells. Each cell in the loops contains one filament, and the filament currents are all assumed to be equal. Then the mutual inductance of this configuration is obtained by the superposition of the mutual

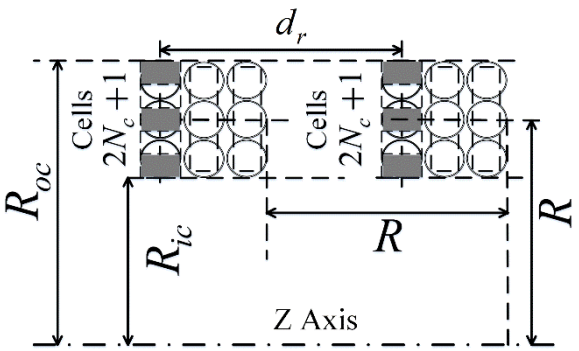

Fig. 5. Configuration of a mesh matrix: loops with multi-layer parallel winding.

inductances of each couple composed by filamentary coils [21]:

$$M_{tt}(R_{ic},R_{oc},d_r)=\sum_{h=-N_c}^{h=N_c}\sum_{l=-N_c}^{l=N_c}M\left(R_h,R_l,d_r\right)\Big/\left(2N_c+1\right)^2 \quad (15)$$

where R_h and R_l are the radius of the corresponding filamentary coils. Here N_c is set to 200, which saves a lot of computing time while the precision is guaranteed.

For a single-layer tightly wound transmitting coil with n_t turns and a radius of R, the overall inductance can be calculated as:

$$L=\sum_{i=1}^{n_t}\sum_{j=1}^{n_t}M\left(R,R,d_{ij}\right)\left(1-\delta_{ij}\right)+\sum_{i=1}^{n_t}L_{si}(R,r_0)$$

$$d_{ij}=\begin{cases}\left|j-i\right|\cdot d_l, & (i-\frac{n_t+1}{2})(j-\frac{n_t+1}{2})<0\\ \left|j-i\right|\cdot d_l+R-n_t d_l/2, & otherwise\end{cases} \quad (16)$$

where d_l is the minimum distance between two consecutive turns, where $\delta_{ij}=1$ for $i=j$ and $\delta_{ij}=0$ for other values. Additionally, the inductance of a transmitting coil with multi-layer parallel winding can be obtained by substituting M_{tt} and L_{sd} into Equ. (16). The gap in a transmitting coil with spaced winding has been limited in Equ. (10). Then considering the gap for d_l, Equ. (16) is still available to derive the inductance of coils with spaced winding. For the topology of multi-wire parallel winding, the coil can be treated as transmitting coils with spaced winding connected in parallel and where coupling factor between them is almost equal to 1. Thus, the inductance of transmitting coils with multi-wire parallel winding is closes to the results of transmitting coils with spaced winding.

B. Stray Capacitance

In the case of transmitting coils with different topologies, the analytical expression of the stray capacitance can be deduced by that of a tightly wound single-layer transmitting coil, which consists of two identical solenoids with $n_t/2$ turns and a stray capacitance that approximates to [15]:

$$C_s=\sum\nolimits_{p<q}C_{p,q}\left(q-p\right)^2\Big/n_t^2 \quad (17)$$

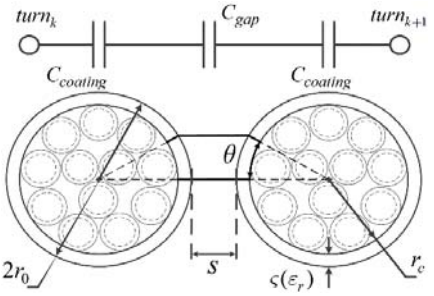

Fig. 6. Equivalent model of the turn-to-turn stray capacitance.

where $C_{p,q}$ is the stray capacitance between turn p and turn q. By only considering the turn-to-turn stray capacitance C_b, a general expression of the stray capacitance C_s can be derived as:

$$C_s=\frac{n_t-2}{n_t^2}C_b \quad (18)$$

As illustrated in Fig. 6, C_b is a combination of stray capacitances through the insulating coatings and air gap. For a single-layer transmitting coil tightly wound with a gap of s between two nearby turns, C_b has been given in [15]:

$$C_b=\varepsilon_0\varepsilon_r\int_0^{\frac{\pi}{4}}\frac{2\pi R r_0}{\varsigma+\varepsilon_r r_0\left(1-\cos\theta\right)+0.5\varepsilon_r s}d\theta \quad (19)$$

where r_0, ς and ε_r are the Litz-wire radius, thickness and relative permittivity of insulting coating, respectively. For multi-wire coils with an arbitrarily number of parallel layers and wires, the voltage differences between the layers or parallel wires can be estimated as zero volts. Then the turn-to-turn stray capacitance of coils with parallel layer and wire winding can be obtained as:

$$C_{bm}=m\sqrt{1+\frac{P_{tc}^2}{4\pi^2R^2}}\cdot C_b \quad (20)$$

where m is the number of parallel layers, and P_{tc} is the pitch of the transmitting coils. Moreover, Equ. (20) is applicable for transmitting coils with the topology of spaced winding. C_s of the transmitting coils reduces with an increase of n_t. However, the effect is reversed for m.

C. AC Resistance of Transmitting Coils

The frequency dependent R_{ac} is determined by the skin and proximity effect losses, and it acts as a major factor to optimize η of WPT systems for EMRs. Usually, Litz-wire is applied to reduce the power losses of the transmitting coils at high frequencies. The skin effect, as well as the proximity effect, can be divided into bundle-level and strand-level in a Litz-wire coil. The bundle-level effect will not be considered in this paper on account of the woven method of Litz-wires, since the current will be distributed equally among the strands [14].

The ac losses of the transmitting coil can be calculated as the sum of the losses in each strand of Litz-wire. To calculate

the skin and proximity effect losses separately, the magnetic field applied to each strand should be uniform and perpendicular to the axis of the bundle, which is consistent with the orthogonality principle [27]. Owing to the symmetry and large dimensions of the transmitting coil, the assumption is satisfied and the ac losses of the transmitting coil are given as:

$$P_t = P_s + P_p = R_{ac} I_m^2 / 2 \tag{21}$$

where I_m is the amplitude of the coil current (assumed to be sinusoidal), P_s is the strand-level skin effect losses, including the dc power losses of the transmitting coil, and P_p represents the strand-level proximity effect losses.

Here, r_s is the radius of strand, n_s is the number of strands in a bundle, and I_m / n_s is the current in each strand. The skin effect losses of each strand within a coil are given by [28]:

$$P_{s\,strand} = \frac{1}{2} R_{s\,strand} \left(\frac{I_m}{n_s} \right)^2 \tag{22}$$

where $R_{s\,strand}$ is the skin effect resistance of a strand:

$$R_{s\,strand} = R_{dc\,strand} \frac{\gamma_s}{2} \frac{ber(\gamma_s) bei'(\gamma_s) - bei(\gamma_s) ber'(\gamma_s)}{ber'^2(\gamma_s) + bei'^2(\gamma_s)}$$

$$\gamma_s = \sqrt{2} r_s / \delta \tag{23}$$

where $\delta = 1/\sqrt{\pi f \mu_0 \mu_r \sigma}$ is the skin depth [29], $R_{dc\ strand}$ is the internal strand dc resistance, and ber, bei, ber', bei' are Kelvin functions.

The strand-level skin effect losses of a coil P_s can be approximated by the sum of the skin effect losses in n_s strands of Litz-wire, and is calculated as follows:

$$P_s = n_s P_{s\,strand} = \frac{1}{2} R_s I_m^2 \tag{24}$$

Then the strand-level skin effect resistance of coil is obtained:

$$R_s = R_{s\,strand} / n_s \tag{25}$$

which indicates that the topology of multi-wire coils with parallel wires and layers connected at both ends reduces R_s by a factor of n_{tw}, the number of wires per turn in the transmitting coils.

Two sources of proximity effects lead to power losses P_p, including H_{int} generated by the adjacent strands of a bundle and H_{ext} caused by nearby bundles. The strand-level proximity losses per unit of length of a round strand are given as [30]:

$$P_{up} = G_s(\gamma_s) \cdot \left(H_{\text{int}} + H_{ext} \right)^2 \tag{26}$$

where:

$$G_s(\gamma_s) = \frac{-2\pi\gamma_s}{\sigma} \frac{ber_2(\gamma_s) ber'(\gamma_s) + bei_2(\gamma_s) bei'(\gamma_s)}{ber^2(\gamma_s) + bei^2(\gamma_s)} \tag{27}$$

in which σ is the conductivity of the strands, and $ber_2(\,)$ and $bei_2(\,)$ are second order kelvin functions. The proximity effect losses of each strand can be achieved by integrating Equ. (26) along a strand, and each strand occupies all of the positions in a bundle. Therefore, a few points need to be noted to simplify the calculation of P_p:

1) Since H_{int} is an uneven function across a section of a bundle and H_{ext} is assumed to be constant over the cross-section of each turn, the internal and external proximity effect losses are orthogonal and can be calculated separately [30]:

$$\left(H_{int} + H_{ext} \right)^2 = H_{\text{int}}^2 + H_{ext}^2 \tag{28}$$

2) The average of H_{int}^2 along the strand is replaced by that over a cross-section of the bundle. Let r_0 be the radius of the bundle. Using Ampere's law, H_{int} at position (ρ, θ) of each strand is obtained as:

$$H_{int} = \frac{I_m}{2\pi r_0^2} \cdot \rho \tag{29}$$

3) H_{ext} over a cross-section of the ith-turn of the transmitting coil should be constant along its length, and is donated as $H_{ext\,i}$.

Thus, the total proximity effect losses can be obtained by the sum of the proximity effect losses in the strands and are simplified as:

$$P_p = \frac{n_s \cdot S_{av} G_s(\gamma_s)}{A_{bundle}} \int_{A_{bundle}} H_{\text{int}}^2 \cdot ds + \sum_{i=1}^{n_t} n_s S_{avi} G_s(\gamma_s) \cdot H_{ext\,i}^2 \tag{30}$$

where $A_{bundle} =$ a cross-sectional area of Litz-wire, S_{av} is the average length of the wire used in the coil, and S_{avi} is the average circumference of the *i*th-turn of the coil. With respect to $H_{ext\,i}$, it can be calculated by static magnetic field formulas [14]. The resistance associated with the proximity effect losses of the transmitting coil can be expressed as:

$$R_p = n_s S_{av} \frac{G_s(\gamma_s)}{8\pi^2 r_0^2} + \sum_{i=1}^{n_t} n_s S_{avi} G_s(\gamma_s) \cdot h_{ext\,i}^2 \tag{31}$$

where $h_{ext\,i}^2 = 2 H_{ext\,i}^2 / I_m^2$, and $h_{ext\,i}$ is defined as the magnetic field generated over the *i*th-turn of the winding when a RMS current of 1 A is circulating in the coil. By giving $H_{ext\,i}$, the R_p of transmitting coils with different topologies can also be obtained with (31).

According to Eqns. (21), (25) and (31), R_{ac} of the transmitting coil is the sum of R_s and R_P. Utilizing analytical expressions of L_s, C_s and R_{ac}, the effects of the topologies on the evaluation parameters of the transmitting coils can be confirmed.

V. Verification with Experiments

Several transmitting coils with different topologies are utilized in this section to validate the analytical model. Then follow-up tests are used to illustrate the feasibility of H_c^2 / R_1 related to η. Apparently, the maximum H_{cd}^2 is applicable to evaluate the power delivered to the receiving side. Notice

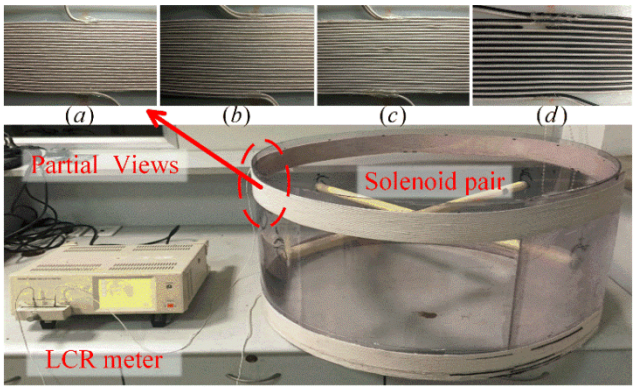

Fig. 7. Experimental setup. (a), (b), (c) and (d) are coils with the topologies in Table I, corresponding to types A, E, B and C.

TABLE I
SPECIFIED TOPOLOGIES FOR TRANSMITTING COILS

Types	NUMBER OF WIRES	Gap	Number of layers
A	1	—	1
B	1	—	2
C	1	*d*	1
D	1	*d*	2
E	2	—	1
F	2	—	2

TABLE II
INDUCTANCE & STRAY CAPACITANCE MEAS. & CALC

Coils	*L CALC. / MEAS.*(mH)	C_s *CALC. / MEAS.*(pF)
A, $n_t = 40$	1.501 / 1.482	12.402 / 12.563
B, $n_t = 40$	1.468 / 1.453	24.804 / 25.134
C, $n_t = 40$	1.332 / 1.321	0.3491 / -
D, $n_t = 40$	1.221 / 1.234	0.6983 / -
E, $n_t = 40$	1.332 / 1.316	12.402 / 12.691
F, $n_t = 40$	1.221 / 1.232	24.804 / 25.437
A, $n_t = 32$	1.019 / 1.047	12.926 / 13.155
B, $n_t = 32$	0.996 / 0.9743	25.852 / 26.092
C, $n_t = 32$	0.923 / 0.9107	0.4306 / -
D, $n_t = 32$	0.877 / 0.902	0.8612 / -
E, $n_t = 32$	0.923 / 0.934	12.926 / 13.232
F, $n_t = 32$	0.877 / 0.913	25.852 / 26.372

that all of the transmitting coils are wound by Litz-wire with 180 strands of AWG38 enameled copper wire, and the diameter of coils is set to 69 cm.

A. *Analytical Model of Transmitting Coils Validation*

R_{es} of the transmitting coil determines η of a WPT system and needs to be accurately predicted by an analytical model, which is first verified in this paper. As shown in Fig. 7, all of the tests are performed using a HIOKI 3532-50 LCR HITESTER equipped with a HIOKI 9260 test fixture. Due to the high voltage gate driver LM5104, the full-bridge inverter adopted in the transmitting circuit has an upper operating frequency limit of around 400 KHz. Therefore, the measurement frequency of R_{es} is kept within the frequency of 500 KHz.

For the topologies of the transmitting coils, there are some restrictions. The diameter of Litz-wire used is 2 cm. First, to make the coil pitch satisfying, the number of parallel wires per turn in the transmitting coils n_w should be not more than 2 and the gap of the spaced coils is set to 2 cm, based on Equ. (10). Second, the large stray capacitance of the transmitting coils with multi-layer parallel winding degrades the high-frequency performance of WPT systems. It is better for the number of layers parallel connected to be limited to 2. The six feasible topologies listed in Table I can be applied to the transmitting coils to optimize the performance of WPT systems. The analytical model suits the single-layer tightly wound transmitting coil, and the number of coil turns has a slight effect on the estimation of R_{es}, which has been validated comprehensively [14]. Thus, tests are performed for transmitting coils with the topologies in Table I, and the number of coil turns is set to 32 and 40.

In Table II, the inductance and stray capacitance of the related transmitting coils are displayed. The stray capacitance of coils with $gap = d$ cannot be measured, which is limited by the measurement frequency range of the LCR meter. The measured results are in accordance with the theoretical analysis, except for the stray capacitance of the transmitting coils with two parallel layers winding. The large difference between them is mainly caused by the uneven distribution of the current within the wires and the manual-winding of the coils.

The transmitting coils wound can be divided by the number of parallel wires per turn and the gap of the spaced winding. In Fig. 8, the calculated and measured R_{es} for each type of transmitting coils are presented: the cases (a), (b) and (c) give the results of transmitting coils with 32 turns, compared with those in the other three of transmitting coils with 40 turns. The test results are similar for all of the transmitting coils, where the calculated R_{es} is in agreement with the measured one at low frequencies and the difference between them becomes larger at high frequencies. The major reason is that the calculation error of the stray capacitance makes the break point of R_{es} to grow up and move to a high frequency. In addition, the large stray capacitance of transmitting coils with fewer turns allows the analytical model to be more reliable. In general, the analytical model gives good predictions for transmitting coils with the selected topologies. However, in other cases, the analytical expression of the stray capacitance should be derived accurately [31].

B. *Evaluation Parameters of Transmitting Coils Validation*

To confirm that H_c^2/R_l is proportional to η, the receiving coil exposed to the same magnetic field intensity

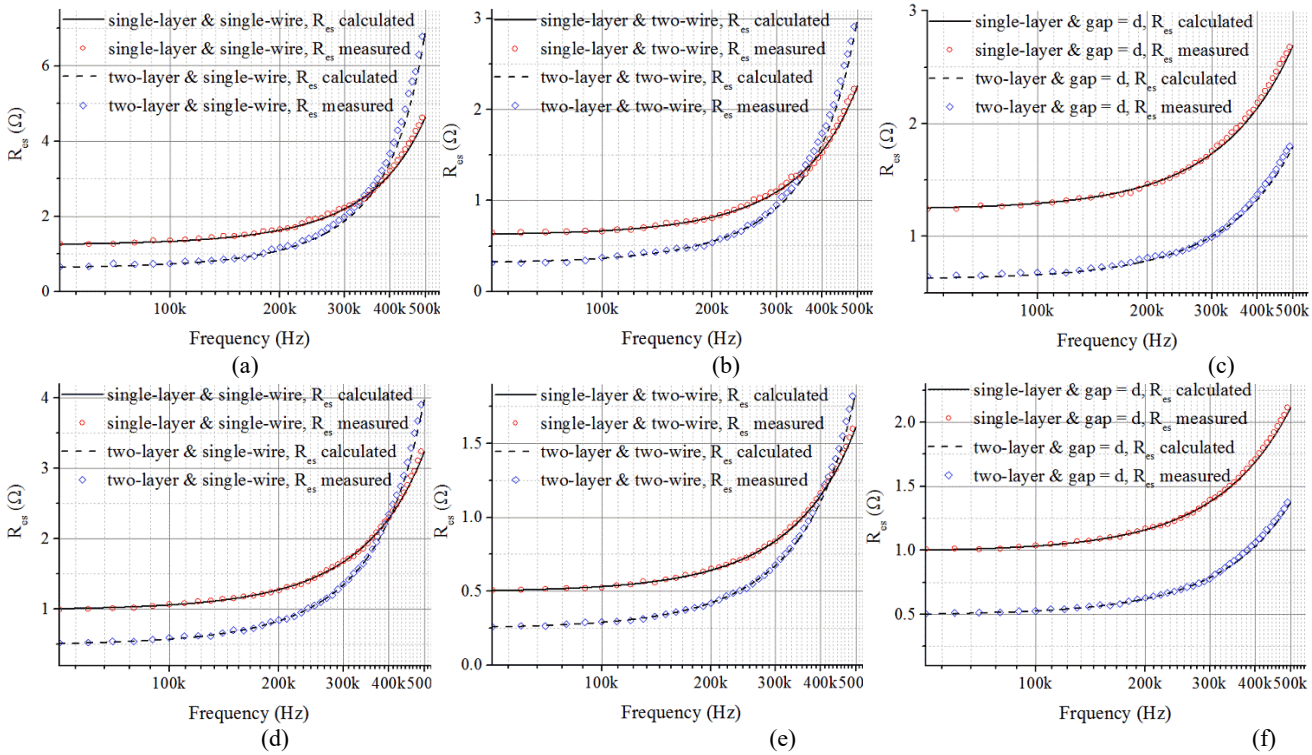

Fig. 8. R_{es} of transmitting coils with the specified topologies in table I. (a), (b), (c) coils with $n_t = 40$; (d), (e), (f) coils with $n_t = 32$.

TABLE III
THE SPECIFICATIONS OF RECEIVING COIL I

Core material	Core dimensions	Coil dimensions
Mn-Zn ferrite R10K	6.5×6.5×6.5 mm	9.5×9.4×10.1 mm

Wire: 12 strands, AWG 44

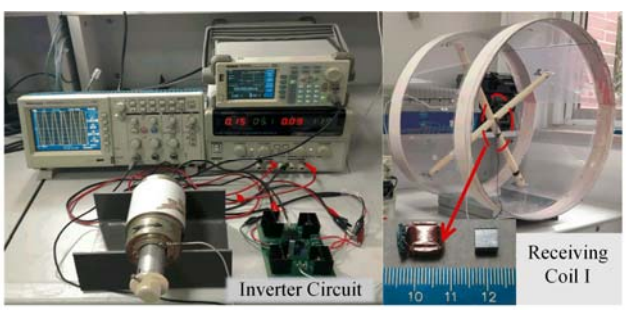

Fig. 9. Experimental setup to test the ability of H_c^2/R_l to evaluate η .

should be located in the workspace of the EMR and axially arranged with the transmitting coils. In accord with the prior optimization analysis [14], receiving coil I loaded with a pure resistance 29.764 Ω is used and placed at the center of the transmitting coils, which are specified in Table III. Meanwhile, the three typical topologies (A), (D) and (F) in Table I are adopted for the transmitting coils. The power transmitted to the receiving side decreases with the number of turns and the number of turns is within the range of 20-60 [14]. Fig. 9 depicts the experiment setup. Keeping the two sides resonant at a frequency of 220 KHz, P_L is measured using an oscilloscope (TDS3052B, Tektronix). R_l has been measured in the case of an inverter circuit loaded with pure resistances at varying frequencies [14]. The power dissipated in the inverter circuit sharply increases as P_L approaches the capacity limit of a WPT system. As seen in Fig. 12 and Fig. 14, for transmitting coils with the selected topologies, a P_L of 200 mW is slightly below the maximum power that can be achieved. Therefore, the measured η of the WPT system in Fig. 10 is obtained when P_L reaches the preset value of 200 mW.

For the different topologies, the calculated H_c^2/R_l in Fig. 13 (a) should be normalized separately according to that of coils with 20 turns to illustrate the relationship between η and H_c^2/R_l . Subsequently, η can be derived by multiplying the normalized results with the measured η of a WPT system for transmitting coils with 20 turns. In Fig. 10, the measured η tends to be consistent with the results derived under the conditions of transmitting coils with a lower number of turns. In addition, the growth rate of η gradually decreases with the number of turns, especially for the single-layer transmitting coil tightly wound. This is because R_l is larger than that measured in [14] and leads to a growth decline of η . However, for transmitting coils with the other topologies, the slowing of the growth rate of η is not so significant.

Regarding the results, two conclusions can be extracted.

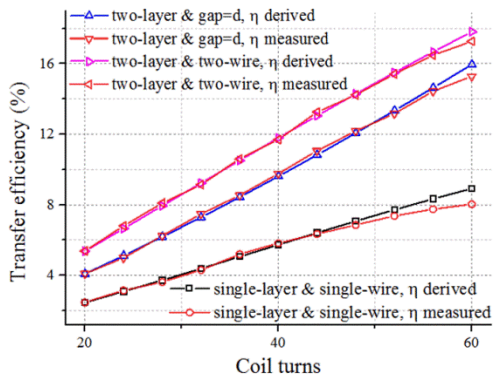

Fig. 10. Derived and measured η of WPT systems varying with n_t, $P_L = 200$ mW. The transmitting coils with the type A, D and F topologies in Table I.

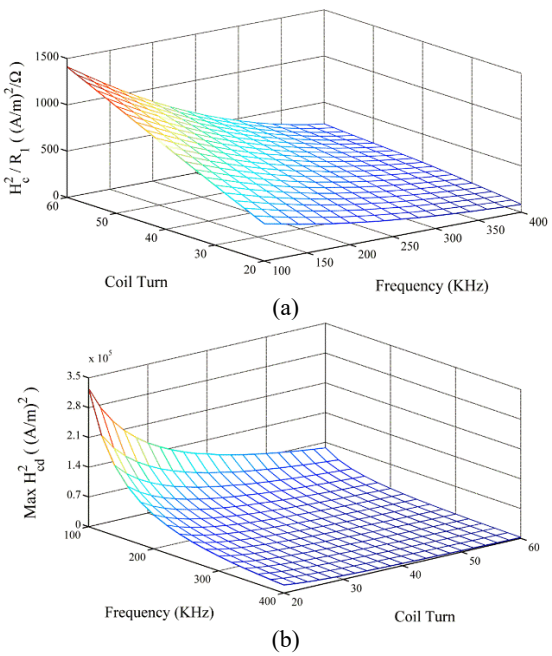

Fig. 11. Simulation results of the evaluation parameters for single-layer transmitting coil tightly wound.

First, keeping the magnetic field around the receiving coil constant, the ratio H_c^2/R_l is linearly related to the η of a WPT system and can be treated as an evaluation parameter. Second, due to the high accuracy of analytical model, the simplified calculation method of H_c, Equ. (9) and (11), is available in the optimal design of transmitting coils with the specified topologies. Being combined with the accurate analytical model, the evaluation parameters proposed can offer proper theoretical guidance for the optimization of the transmitting coil.

VI. Standardized Design

As a platform for EMR systems, a suitable topology for the transmitting coil can be determined by the calculated results of H_c^2/R_l and the maximum H_{cd}^2 to provide sufficient energy for the EMR system. Then it is confirmed with experiments in this section.

A. Topologies Theoretically Selected for Transmitting Coils

In this sub-section, the optimal topology of a transmitting coil is determined in theory with the evaluation parameters: H_c^2/R_l and the maximum H_{cd}^2. Being in series resonance with the transmitting coils, the voltage across the turning capacitor is Q_l times the input voltage of the transmitting circuit. The rated voltage of the vacuum turning capacitor is 7.5 KV (CKTB1000/7.5/100). Thus, I_d of the transmitting coils should be less than $7500/Q_l \cdot R_l^{-1}$ A, which limits the maximum H_{cd}^2 of the coils. For single-layer transmitting coils tightly wound, the tendency of the evaluation parameters to vary with the frequency and the number of turns has been specifically depicted in Fig. 11. The calculated results reveal that H_c^2/R_l decreases with the frequency, but greatly increases with the number of turns. However, the maximum H_{cd}^2 decreases with the frequency and the number of turns separately. In the case of different topologies, the evaluation parameters of the coils follow a similar trend. In addition, the topologies just enlarge H_c^2/R_l of the coils within the applicable frequency ranges, which are slightly affected by the number of turns.

To compare the performance of transmitting coils with the selected topologies, the number of turns is set to 40. In this case, instead of H_{cd}^2, the maximum I_d is utilized to illustrate the power transmitted to the receiving side and it is closely related to L_s of transmitting coils in Equ. (12). Because of a slowly changing L_s with the frequencies in Fig. 12(b), some curves of the maximum I_d overlap for different topologies. The results in Fig. 12 indicate that transmitting coils with multi-layer parallel winding merely improve the performance of WPT systems in the low frequency range. In addition, transmitting coils with multi-wire parallel winding can be applied widely. Moreover, especially at high frequencies, transmitting coils with spaced winding are suitable for high-power WPT systems. At a frequency of 220 KHz, the application of the topology of two-layer and two-wire parallel winding to transmitting coils can greatly improve η of a WPT system. Actually, the maximum H_{cd} generated by transmitting coils is more crucial in the WPT systems for EMRs. Therefore, the spaced transmitting coil with two-layer parallel winding is still available.

The number of turns has to be considered to determine the optimal topology for the transmitting coils. Varying with the number of turns, the impact of transmitting coils with the two optional topologies on the performance of WPT systems is theoretically analysed and shown in Fig. 13 at the operating

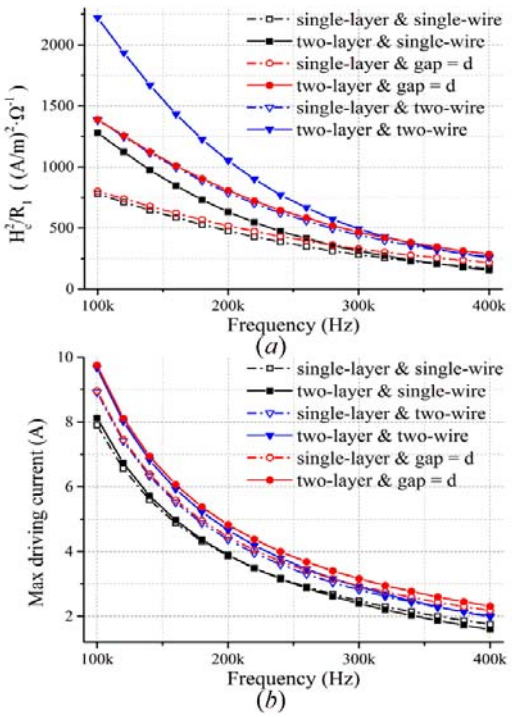

Fig. 12. The calculated H_c^2/R_1 and the max I_d versus the frequency for transmitting coils with $n_t = 40$ and the topologies specified in Table I.

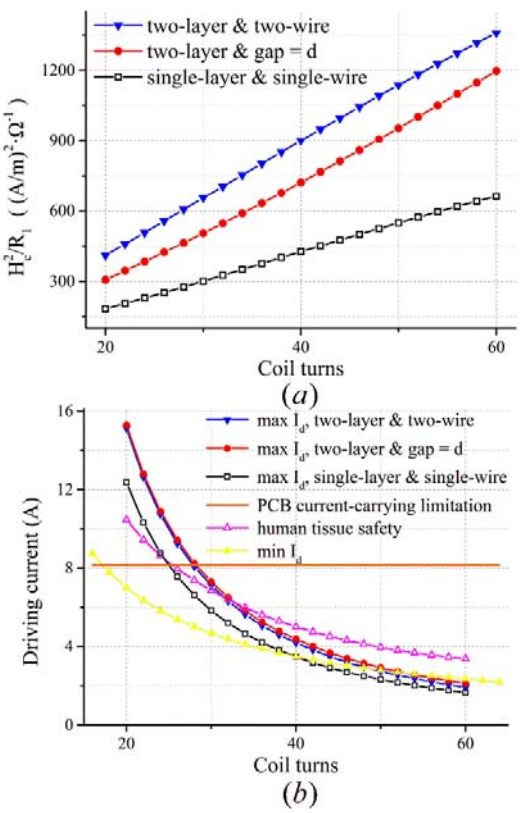

Fig. 13. The calculated H_c^2/R_1 and the permissible I_d varying with n_t at 220 KHz for transmitting coils with the type A, D and F topologies in Table I.

frequency. Due to a small difference in the maximum I_d, a transmitting coil with two-layer and two-wire parallel winding realizes a better performance. Once the topology of a transmitting coil is determined, on the premise of satisfying the power demand of an EMR system, the number of turns can be selected to improve η as much as possible.

As a rule, I_d is also restricted by other factors, which has been clearly explained in [14]. First, based on the generic standard on the printed board design IPC-2221A, the maximum current load of the tracks is set to 8.16 A given a safety factor of 50%. Second, because of the restriction of the International Commission on Non-ionizing Radiation Protection (ICNRP 1998), the limits of I_d can be obtained through the numerical simulation method in [12] to maintain human tissue safety. Last, the minimum I_d for the transmitting coils should ensure a magnetic field intensity of 0.2104 mT at the workspace of an EMR to achieve P_L of 500 mW for an EMR system with receiving coil I internally installed [12]. All the constraints have been shown in Fig. 13(b).

The maximum I_d should be higher than that restricted by human tissue safety to prevent the vacuum turning capacitor from continually operating beyond its nominal voltage. The larger the number of turns, the higher H_c^2/R_1 becomes. Thus, the number of turns is set to 30. At this point, as seen in Fig. 13(a), the re-optimized transmitting coil can theoretically improve η of WPT systems from 3.55% to 8.42% when compared with a single-layer transmitting coil tightly wound with 28 turns [14].

B. Topologies Further Confirmed via Experiments

The optimal topology of the transmitting coil has been selected by simulation, and needs to be verified to confirm the amount of power delivered to the load of the receiving side under the influence of a normal working environment. The experimental setup is the same as the tests in Section V. B.

To illustrate the effect of the selected topology on the performance of WPT systems, single-layer transmitting coils tightly wound are utilized. Considering the limits of I_d in Fig. 13(b), the maximum P_L is measured for transmitting coils with the two topologies, and presented in Fig. 14. The varying tendency of the maximum P_L is similar to that of the derived maximum I_d, which indicates that the analytical model has higher reliability and precision. In [14], for single-layer transmitting coils tightly wound, the optimal number of turns is set to 28. In addition, the maximum P_L is about 750 mW at a η of 3.58% as shown in Fig. 14. By contrast, a transmitting coil with the optimal topology improves the performance of the WPT system. When setting

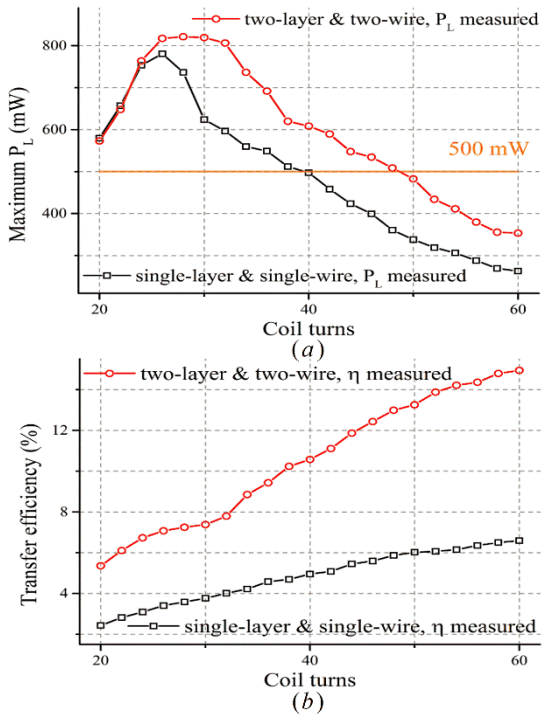

Fig. 14. Measured maximum P_L and associated η varying with n_t at 220 KHz for transmitting coils with the type A and F topologies in Table I.

the number of turns to 30, the maximum H_{cd} was the setup value required by human tissue safety. Thus, due to its high permeability, the ferrite core of receiving coil I was magnetically saturated, and a P_L of 819.36 mW can be realized at a η of 7.37%, which is less than a η of 8.549% in case of a P_L of 200 mW. The decreasing η was mainly caused by increasing of R_1. Compared with the previous studies, η of the WPT system was increased from 3.58% to 7.37% through the re-optimization of the transmitting coils in [14], which is much higher than a η of 4.08% for the WPT system with a transmitting range of 20 cm [12]. Adopting the topology of multi-wire coil with two-layer and two-wire parallel connected at both ends, a transmitting coil with turns 30 can acts as a platform to supply sufficient power for most EMR systems.

Due to the limited space for the receiving coils, the inductive coupled WPT system cannot be applied to high-power EMR systems. If the power requirements of EMR systems are satisfied, the optimization of transmitting coils is worthwhile and meaningful.

C. Standardized Design of Transmitting Coils

Based on the re-optimization of the above transmitting coil, the optimization process of the transmitting coil in the WPT systems for EMRs through adjusting the topology is obtained and standardized as shown in Fig. 15. The flowchart includes two parts. The design constraints and requests of the

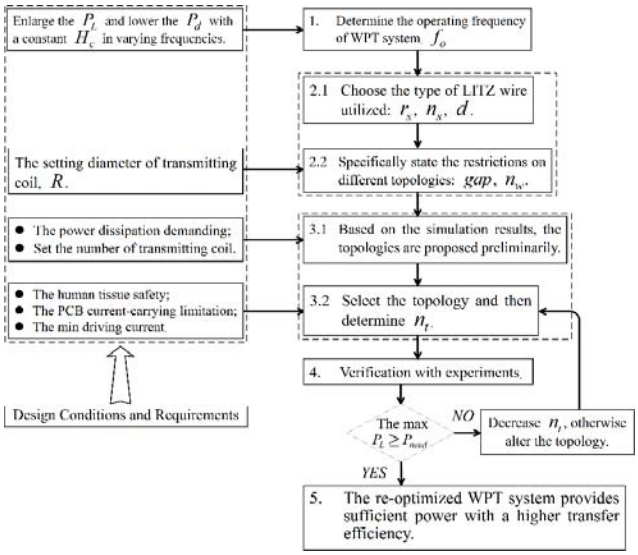

Fig. 15. Design optimization flowchart of the transmitting coils in the WPT systems for EMR systems.

transmitting coil all depending on the receiving side of the WPT systems and the power demand of the EMR systems. Next, the implementation of the transmitting coil with the optimal topology and number of turns by enlarging η with modelling and experiments on the basis of an adequate power supply for EMR systems.

Some of the typical receiving coils installed in EMRs have been thoroughly studied and optimized. Thus, in step 1, the f_o of WPT systems has to be determined by the receiving sides to increase P_L and to reduce the amount of power dissipated in the receiving sides P_d through tests. To simplify the analysis, the external magnetic field intensity around the receiving coils remains the same with a varying operating frequency that can be achieved by the drive circuit of the transmitting sides. Then the P_L and P_d of typical receiving coils under specific loads are measured. A higher P_L ensures the normal work of EMR systems and lowers the amount of power absorbed by human tissues. However, P_d should be relatively small to avoid a large temperature rise in the receiving coils. Therefore, depending on the power demand of EMR systems, f_o is set to a frequency at which the EMR can operate stably and reliably [14]. The primary benefit of Litz-wire is the reduction of ac losses. In Litz-wire selection, f_o influences the actual Litz construction, and is used to determine the wire gauge of each strand. From empirical data, the optimal wire gauge r_s at the frequency of f_o has been given by the manufacturers. Litz-wire constructions vary from just a bunch of strands to complex designs utilizing multiple cores and several manufacturing operations. All of them have their own applications, such as in high Q circuitry or tuning circuitry. After determining of

the Litz-wire type, a Litz-wire with a larger n_s in the restricted product list will be adopted in step 2.1 on the premise of limited costs [32]. In the case of a transmitting coil with the shortest length permitted by experience, the maximum pitch is obtained with a numerical analysis to diminish the impact of H_{cr} to the extent set. Therefore, the design parameters gap and n_w are provided.

The rest of steps in Fig. 15 are specific to the optimization of transmitting coils conducted by simulation and experiment. It is generally true that a larger number of layers in multi-wire transmitting coils leads to a drastic decrease in the self-resonant frequency. As a result, R_{es} increases a great deal around the frequency of f_o. Meanwhile, R_{es} can be accurately obtained by the analytical mode. In step 3, the number of parallel layers in multi-wire transmitting coils is limited to guarantee a considerable decrease of R_{es}. Then all of the available topologies of transmitting coils are specified. Step 3.1 sets the number of turns in the transmitting coils to a certain value, and the evaluation parameters are achieved by calculations at different frequencies. Suitable topologies for the transmitting coils to improve η or P_L are primarily decided at the frequency of f_o. In step 3.2, considering the limits of I_d that vary with the number of turns, the optimal topology and number of turns are theoretically determined to meet the requirements of EMR systems. Later, the theoretical results are verified in step 4 with experiments to illuminate the maximum P_L. Moreover, if the maximum P_L is less than the power demand of EMR systems, the number of turns has to be reduced to improve H_{cd}. However, this is only feasible when the maximum I_d is less than the limitations set by the human tissue safety and PCB current-capacity. Finally, the WPT system with the transmitting coil optimized is able to provide sufficient power with higher efficiency for EMR systems.

VII. Results and Conclusion

Transmitting coils can be optimized with the topologies of spaced winding and multi-wire coils with parallel wires connected at both ends. To evaluate the effect of transmitting coils on the performance of WPT systems, H_c^2/R_1 and maximum H_{cd}^2 have been derived and experimentally verified. In case of a constant H_{cd} for the receiving coils, H_c^2/R_1 is in proportion to η of WPT systems. Additionally, based on a numerical analysis, the maximum pitch of the transmitting coils has been restricted to ensure the uniformity of H_c.

To facilitate the optimization design, an analytical model of transmitting coils has been built. Although the calculation error of stray capacitance is distinct, the analytical model can still accurately predict the evaluation parameters of transmitting coils with the specified topologies. The calculated results of the evaluation parameters indicate that the transmitting coil with spaced winding is suited for high-power WPT systems especially at high frequencies. In addition, the topology of multi-wire parallel winding can be used over a wide frequency range. However, the topology of multi-layer parallel winding only applies to transmitting coils at low operating frequencies. At 220 KHz, the topology of two-layer and two-wire parallel winding is optimal for the transmitting coil in [14], and its number of turns is set to 30. The practical results show that the maximum P_L of 819.36 mW is obtained at an η of 7.37%. Since the maximum H_{cd} exceeds the restrictions of ICNRP, the re-optimized coil can act as a platform for most EMR systems. Furthermore, the standardized design of the transmitting coil is obtained by summarizing, which is effective when the diameter of the transmitting coil or f_o varies.

References

[1] G. Iddan, G. Meron, and P. Swain, "Wireless capsule endoscopy," *Nature*, Vol. 405, No. 6785, pp. 417, May 2000.

[2] S. Bang, J. Y. Park, S. Jeong, and Y. H. Kim, "First clinical trial of the "MiRo" capsule endoscope by using a novel transmission technology: electric-field propagation," *Gastrointest. Endosc*., Vol. 69, No. 2, pp. 253-259, Feb. 2009.

[3] D. R. Cave, D. E. Fleishcer, and J. A. Leighton, "A multicenter randomized comparison of the Endocapsule and the Pillcam SB," *Gastrointest Endosc*., Vol. 68, No. 3, pp. 487-494, Sept. 2008.

[4] H. M. Kim and Y. J. Kim, "A pilot study of sequential capsule endoscopy using MiroCam and Pillcam SB devices with different transmission technologies," *Gut Liver*, Vol. 4, No. 2, pp. 192-200, Jun. 2010.

[5] A. Moglia, A. Menciassi, P. Dario, and A. Cuschieri, "Capsule endoscopy: progress update and challenges ahead," *Nature Reviews Gastroenterology & Hepatology*, Vol. 6, No. 6, pp. 353-361, Jun. 2009.

[6] A. V. Gossum and M. Ibrahim, "Video capsule endoscopy: what is the future?," *Gastroenterology Clinics of North America*, Vol. 39, No. 4, pp. 807-826, Dec. 2010.

[7] P. Swain, "The future of wireless capsule endoscopy," *World J Gastroenterol*, Vol. 14, No. 26, pp. 4142-4145, Jul. 2008.

[8] M. Ryu, J. D. Kim, H. U. Chin, J. Kim, and S. Y. Song, "Three-dimensional power receiver for in vivo robotic capsules," *Med. & Biol. Eng. & Comput*., Vol. 45, No. 10, pp. 997-1002, Oct. 2007.

[9] R. Carta, "A wireless power supply system for robotic capsular endoscopes," *Sensors and Actuators A: Physical*, Vol. 162, No. 2, pp. 177-183, Aug. 2010.

[10] W. Xin, G. Yan, and W. Wang, "Study of a wireless power transmission system for an active capsule endoscope," Int. *J. Med. Robot. Comput. Assist. Surg*., Vol. 6, No. 1, pp. 113-122, Jan. 2010.

[11] W. Chen, G. Yan, P. Jiang, and H. Liu, "A wireless capsule robot with spiral legs for human intestine," *Int. J. Med. Robot. Comput. Assist. Surg*, Vol. 10, No. 2, pp. 147-161, Jun. 2014.
[12] Z. Jia and G. Yan, "The optimization of wireless power transmission: Design and realization," *Int. J. Med. Robot. Comput. Assist. Surg*., Vol. 8, No. 3, pp. 337-347, Sep. 2012.
[13] S. He, G. Yan, Q. Ke, and Z. Wang, "A wirelessly powered expanding-extending robotic capsule endoscope for human intestine," *International Journal of Precision Engineering and Manufacturing*, Vol. 16, No. 6, pp. 1075-1084, Jun. 2015.
[14] Q. Ke, W. Luo, G. Yan, and K. Yang, "Analytical model and optimized design of power transmitting coil for inductive coupled endoscope robot," *IEEE. Trans. Biomed. Eng*., Vol. 63, No. 4, pp. 694-706, Apr. 2016.
[15] Z. Yang, W. Liu, and E. Basham, "Inductor modeling in wireless links for implantable electronics," *IEEE Trans. Magn*., Vol. 43, No. 10, pp.3851-3860, Oct. 2007.
[16] S. Y. R. Hui, W. Zhong, and C. K. Lee, "A critical review of recent progress in mid-range wireless power transfer," *IEEE Trans. Power Electron*., Vol. 29, No. 9, pp. 4500-4511, Sep. 2014.
[17] C. Peter and Y. Manoli, "Inductance calculation of planar multi-layer and multi-wire coils: An analytical approach," *Sensors and Actuators A: Physical*, Vol. 145-146, pp. 394-404, Jul. 2008.
[18] P. T. Theilmann and P. M. Asbeck, "An analytical model for inductively coupled implantable biomedical devices with ferrite rods," *IEEE Trans. Biomed. Circuits Syst*., Vol. 3, No. 1, pp. 43-52, Feb. 2009.
[19] C. M. Zierhofer and E. S. Hochmair, "Geometric approach for coupling enhancement of magnetically coupled coils," *IEEE Trans. Biomed. Eng*., Vol. 43, No. 7, pp. 708-714, Jul. 1996.
[20] S. Babic and C. Akyel, "Improvement in calculation of the self- and mutual inductance of thin-wall solenoids and disk coils," *IEEE Trans. Magn*., Vol. 36, No. 4, pp. 1970-1975, Jul. 2000.
[21] K. B. Kim, E. Levi, Z. Zabar, and L. Birenbaum, "Mutual inductance of noncoaxial circular coils with constant current density," *IEEE Trans. Magn*., Vol. 33, No. 5, pp. 4303-4309, Sep. 1997.
[22] G. Ma, G. Yan, and X. He, "Power Transmission for Gastrointestinal Microsystems using Inductive Coupling," *Physiol. Meas*., Vol. 28, No. 3, pp. N9-N18, Mar. 2007.
[23] S. She, "Simple formulas for analyzing magnetic field homogeneity of helmholtz coil helical solenoid and circular loop," *College Physics*, Vol. 18, No. 8, pp. 1-3, Aug. 1999.
[24] E. L. Bronaugh, "Helmholtz coils for calibration of probes and sensors: limits of magnetic field accuracy and uniformity," in *Proc. IEEE Int. Symp. Electromagn. Compat.*, pp. 72-76, Aug. 1995.
[25] W. Feng, "Numerical calculation of magnetic field distribution along axis of a helical current," *College Physics*, Vol. 21, No. 3, pp. 31-33, Mar. 2002.
[26] L. Wang, "Calculation and measurement of Solenoid inductance," *Electrical Measurement & Instrumentation*, No. 11, pp. 12-16, Nov. 1982.
[27] J. A. Ferreira, "Improved analytical modeling of conductive losses in magnetic components," *IEEE Trans. Power Electron*. Vol. 9, pp. 127-131, Jan. 1994.
[28] J. A. Ferreira, *Electromagnetic Modeling of Power Electronic Converters.* Boston, MA: Kluwer, 1989, pp. 88.
[29] M. K. Kazimierczuk, *High-Frequency Magnetic Components*, 2th ed., John Wiley & Sons, Ltd, 2014, pp. 167.
[30] J. A. Ferreira, "Analytical computation of AC resistance of round and rectangular litz wire windings," *IEE PROCEEDINGS-B*, Vol. 139, No. 1, pp. 21-25, Jan. 1992.
[31] A. Massarini et al., "Self-capacitance of inductors," *IEEE Trans. Power Electron*. Vol. 12, No. 4, pp. 671-676, Jul. 1997.
[32] New England wire, http://www.newenglandwire.com, 2016.

Quan Ke was born in Hubei, China, in 1989. He received his B.S. degree from Changchun University, Jilin, China, in 2011; and his M.S. degree in Instrument Science and Engineering from Shanghai Jiaotong University, Shanghai, China, in 2013. He is presently working towards his Ph.D. degree in the Institute of Precise Engineering and Intelligent Microsystems, Shanghai Jiaotong University. His current research interests include wireless power transfer and equipment for medical treatment.

Pingping Jiang was born in Anhui, China, in 1975. She received her B.S. and M.S. degrees from the Hefei University of Technology, Anhui, China, in 1997 and 2000, respectively; and her Ph.D. degree in Instrument Science and Engineering from Shanghai Jiaotong University, Shanghai, China, in 2005. Since 2000, she has been with Shanghai Jiaotong University, where she is presently working as an Associate Professor in the Department of Instrument Science and Engineering. Her current research interests include intelligent measurement systems and biomedical signal processing.

Guozheng Yan received his Ph.D. degree in Engineering from Jilin University, Jilin, China, in 1993. Since 1996, he has been with Shanghai Jiaotong University, Shanghai, China, where he is presently working as a Professor and Head of the Institute of Precise Engineering and Intelligent Microsystems. His current research interests include intelligent robots and micro electromechanical systems.